EUROPEAN
ACADEMIC
RESEARCH

Gap Energy Calculation of Nanometric ZnO Particles via High Energy Grinding

BARBOSA, DA COSTA BARBOSA
Mechanical Engineer of
Embedded Systems Laboratory at Amazonas State University, Brazil
CISNEROS, EDRY ANTONIO GARCIA[1]
Doctor, Professor of Mechanical Engineering at Amazonas State University, Brazil
DE SOUZA SERGIO MICHELON
Doctor, Professor of Physics at the Federal University of Amazonas
HAPUQUE, QUEREM FELIZ RABELO
Doctor, Professor of Physics at the Federal University of Pará

Abstract

Mechanical alloying is a high energy ball milling technique involving cold welding and fracturing in a high energy mill. Known for a long time in metallurgy, this technique presents favorable results with materials with improved structural and mechanical properties and with superior performance to other conventional processes. The present work describes the production of nanostructured ZnO via high energy milling with different steel spheres. The samples were characterized by X-ray diffraction for crystallite size studies and by UV-Vi's spectrophotometry for Gap energy calculation. Gap energy was calculated using the McLean equation. The results of the work allowed us to state that the average sizes of crystallites calculated for the Lorentizian, Gaussian and Pseudo Voigt functions were very close, that is, considering different diameters of grinding spheres, there are no variations in crystallite sizes when the BPR is kept fixed in the milling process. The absorbance measurements for commercial ZnO particles allowed a direct gap calculation of the samples through the McLean equation.

Keywords: Gap Energy

1. INTRODUCTION

The study of nanoscale materials has been growing almost exponentially in the scientific community in various fields of science. Exploring more and more the materials in the scale between 1 to 100 nm gives us the possibility to obtain new properties and applications for nanotechnology [1-2].

---

[1] Corresponding author: edry1961cu@gmail.com

ZnO is a very interesting material due to its numerous applications, easy synthesis process and in nanostructured form presents modified properties many of the times better than the material in its micro structured form [3].

Making an analysis on the website http://www.sciencedirect.com it is possible to observe a marked increase in the number of articles that address the theme of obtaining and applying zinc oxide this theme. See figure 1.

Figure 1: Yearly increase in the number of articles on zinc oxide.
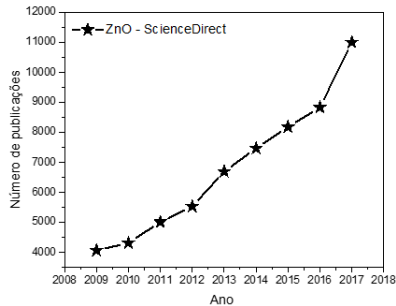
Source: Authors, 2017

Regarding the properties of this material, it is possible to state that it is a nano material, has many possibilities for applications in non-electronics, and photonics, is very resistant to radiation, has piezoelectric, ferroelectric, ferromagnetic properties, is a cheap material, non-toxic, with high electrical conductivity and transparent in the visible range.

Some authors report in the literature applications of this nano material, above all, in the areas of active components, electronic, optical, electrochemical, and electromechanical devices, light emitting diodes (LED's), field effect transistor (FET's), chemical and biological sensors, photodetectors, electron emitters among others [3-6]. See figure 2.

The present work describes the production of nano structured ZnO via high energy milling with different steel balls (diameter 2, 4, 6 and 8 mm). The samples were characterized by X-ray diffraction for crystallite size studies and by UV-Vis spectrophotometry for Gap energy calculation. The general objective of this research was to calculate gap energy for ZnO samples nanometrized by the mechanical milling process.

Figure 2. Example of many aplications of ZnO

Source: Azuma E. D, (2016).

The results obtained allowed us to demonstrate that high-energy grinding on ZnO particles produced nanostructured samples for different bead diameters.

2. Development

Zincite (ZnO)

ZnO has three types of crystal structures wurtzite, zinc blende and rock-salt. The thermodynamically most stable phase is Wurtzite with Hexagonal structure, space group P 63/mc. The optical and electrical properties of the Wurtzite phase depend on the amount of oxygen in the structure.

X-ray diffraction technique is a very effective technique to determine network parameters with Zn saturation [7].

Figure 3 Crystal structure of ZnO (Wurtzite).
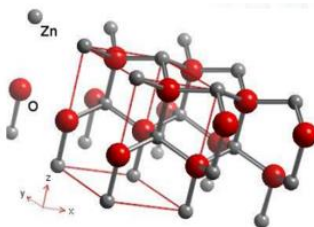
Source: Reisdoerfer, E.C, (2008)

The $[Zn]_{(1+x)}$ O is a non-stoichiometric compound with excess interstitial Zn2+ cations and free electrons. The ionic radii of Zn2+ are larger and tend to increase the deviation from the ideal anion-cation ratio, this is because the ionic radii of Zn2+ have sufficient dimensions to be coordinated by six O-2 anions. According to Reisdoerfer (2008), the bonds in ZnO are 50-60% ionic and the dominant defects are interstitial zincs due to excess.

The possible photoluminescence (PL) emission at approximately 2.5 eV (approximately 495 nm), originating from intrinsic defects, makes ZnO suitable for applications in field emission and vacuum fluorescent displays [8].

Mechanical Grinding

Mechanical alloying is a high energy ball milling technique involving cold welding and fracturing in a high energy mill. Known for a long time in metallurgy, this technique results in materials with improved structural and mechanical properties and with performance superior to other conventional processes. During mechanical grinding we can reduce particle sizes of materials, but the process as a whole offers low commercial values because the energy used in the process is very high and much of it is converted into heat [9-10].

The mechanical grinding technique was developed by John S. Benjamin and his colleagues at the Paul D. Merica Research Laboratory at INCO [14]. Figure 4 illustrates the development period of the mechanical milling process. In 1966, nickel alloys were already being produced by mechanical milling for industrial needs, followed by the production of oxide alloys with strengthened superalloys (oxide dispersion strengthened - ODS) used in the Gulf War by the United States. As of 2000 many publications already considered mechanochemical processes, which allowed a prediction of the resulting phases through the process. In 2001 the search for applications of materials synthesized by mechanical milling began, in this period the materials produced presented metastable phases or nanoscale structures [11-15].

Ball milling allows the production of crystalline, amorphous and nano structured materials through the collisions of balls with the powders and with the walls of the milling jar [16]. In general terms, this process occurs when the high purity powders used in the process are submitted to a cold-welding process, followed by re-welding, through the transfer of mechanical energy from the collisions with the particles, resulting in a powder with a high degree of defects having its grain size minimized [17].

MAE is a solid-state powder processing technique that involves cyclically repetitive fracturing and welding of the powder particles in a high-energy ball mill to produce a homogeneous material [18]. MAE is a method of producing nanostructured metals and metal alloys due to its ability to produce large-scale materials employing relatively simple equipment and at room temperature.

The term high-energy milling is employed to differentiate the family of milling processes from conventional processes such as vibratory mill milling, planetary mill and attritor (Szegvari type) milling.

X-Ray Diffraction

If under a crystal the incident radiation of wavelength similar to the spacing of the crystal scatters, then we have the phenomenon of diffraction. The diffracted rays on a set of planes defined by Miller indices (hkl) are defined by Bragg's Law, according to equation (I)

$$n\lambda = 2d_{hkl}\sin\theta \qquad (I)$$

where λ is the wavelength of the radiation, n is the order of reflection and can be any integer (1, 2, 3, ...), d_hkl is the Inter planar distance of the crystallographic planes and θ is the diffraction angle (or Bragg angle). In X-ray diffraction, Bragg's law relates the wavelength, the position of the Bragg peak and the distance between the crystallographic planes.

Figure 4. Illustration of Bragg's Law.
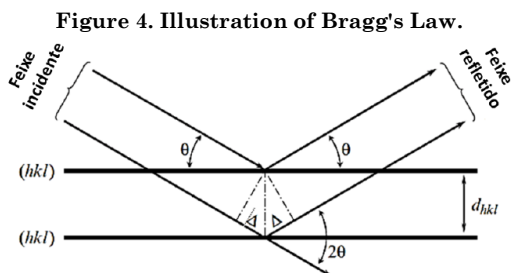
Source: SUWANBOONA, S. and AMORNPITOKSUKB, P. 2012.

The diffraction pattern of the samples has unique diffraction peak intensities and positions for each substance, allowing analysis of the phases present [19].

Average crystallite size using XRD

To analyze the crystallite size, we should consider the instrumental broadening, because its contribution is quite means in the crystallite size and microvoltage broadening in the diffraction peaks. According to Scherrer's equation, we have:

$$t_c = \frac{K\lambda}{\beta\cos\theta} \qquad (II)$$

where K is Scherrer's constant or proportionality constant that depends on the crystal shape and size distribution, ß is the peak width, better known as FWHM (Full Width at Half Maximum). As the crystallite size decreases, the peak gets wider and for large angles we can also see that the widening of the crystallite size is more pronounced, however the intensity of the peak is generally weaker at larger angles.

This equation was developed in 1918 by P. Scherrer under ideal conditions for cubic crystals with perfectly parallel planes in monochromatic X-ray beam was scattered in the crystal. Equation (I) relates the peak width to the crystallite size, that is the set of crystalline planes that contribute to

the diffraction in that direction. The peaks also relate the structural aspects of the sample (line shapes).

Although the shapes of crystallites are generally irregular, we can often approximate them as: sphere, cube, tetrahedron, octahedron, parallelepiped, prism or cylinder. Most applications of Scherrer analysis assume spherical crystallite shapes. If we know the shape of the crystallite from another characterization measurement, we can use the appropriate value for the Scherrer constant.

According to Scott in his lecture notes (Available at http://prism.mit.edu/xray), the values of K can be:

K = 0,91 no crystal information (good approximation)

K = 0.89 for spherical particles with cubic symmetry;

K = 0.73 to 1.03 for crystals with tetrahedral symmetry;

K = 0.82 to 0.94 for crystals with octahedral symmetry;

K = 0.82 <K <1.03 are the typical extremes.

For the calculations of average crystallite sizes in this research a value of 0.91 was considered for the Scherrer constant.

There are several factors that can influence the average crystallite size. They are: peak convolution, wavelength width of the Kα and Kβ lines, size of the X-ray source, overlap of Kα and Kβ peaks, beam divergence, slit width, imperfect concentration, beam size, beam penetration into the sample, among others.

Ultraviolet-Visible Spectroscopy (UV//Vis)

The absorption process, observed in spectrometers, follows the principles of Beer-Lambert's law, where the inter-relationship between the degree of attenuation, the concentration of absorbing molecules in the material and the length of the optical path over which absorption occurs is observed in a quantized manner. This attenuation can be represented by Figure 13 (a), where a monochromatic beam of intensity I_0 is directed to a solution of adsorbent material with thickness b, in cm, and concentration c, in moles per liter (SKOOG et al., 2006). As it travels along path b the intensity of the beam decreases from I_0 to I. The fraction of I_0 transmitted through the solution is called Transmittance (T) and expressed according to equation (III):

$$T = \frac{I}{I_0} \qquad\qquad (III)$$

The absorbance (A) is related in a logarithmic way to the Transmittance (T) values, following equation (IV):

$$A = -\log T = \log \frac{I_0}{I} \qquad\qquad (IV)$$

The absorbance values of a material are expressed by means of an absorbance spectrum as shown in Figure 13 (c).

When measurements are desired in a UV/Vis spectrophotometer, the sample must be contained in containers (quartz or glass cuvettes). However, this entrapment causes some losses by scattering or reflection of the beam. In addition, scattering losses can occur due to undesirable particles such as dust. In order to minimize these losses, it is adopted the similarity between the values of transmitted beam intensity (and hence Transmittance) with the intensity values observed when passing through a cuvette filled only with solvent or reagent blank:

$$A = \log \frac{I_0}{I} \approx \log \frac{I_{solvente}}{I_{solução}} \qquad (V)$$

Applying Beer-Lambert's law we have

$$A = \log \frac{I_{solvente}}{I_{solução}} = \alpha bc \qquad (VI)$$

where A is the absorbance, α is the molar absorptivity, b is the optical path taken by the UV/Vis beam, and c is the solute concentration.

Gap Energy of Semiconductors

In crystalline solids there are certain bands of allowed energies, separated by bands of forbidden energies, that is, energies that the electrons cannot assume.

Two bands are quite important: the band of electrons strongly attached to covalent bonds, called the valence band, and the band of valence electrons that have become free electrons, and is called the conduction band.

For semiconductors there is also a forbidden band, but it is much narrower when compared to insulators. At very low temperatures, semiconductors behave like insulators, because their electrons do not have enough energy to move into the conduction band.

In a semiconductor the gap energy has a reasonable value that can often be obtained through electromagnetic radiation (light) or thermal energy. In other cases we have that to promote the facilitation of the conduction band carriers it is necessary to add impurities so that the energy within the forbidden band is facilitated and then promoted to conduction band carriers, this possibility occurs through doping.

Direct energy gap semiconductors are generally characterized by a high absorption coefficient in the energy range relevant for photovoltaics; most sunlight is absorbed within a small band below the surface; the possibility to fabricate thin-film solar cells.

Indirect gap semiconductors, on the other hand, need more material to absorb most of the sunlight:

- Addition of metals like Si and Ge among others;
- When in solar cells thick layers are needed;
- Higher material costs and increased demand on purity.

Absorption spectroscopy is an interesting technique for exploring optical properties of semiconductor materials.

The optical band gap is determined from the absorption spectrum using via McLean's analysis [32]:

$$(\alpha h v) = A(h v - E\_g)^{(1/n)} \qquad (VII)$$

where α is the absorption coefficient, h is the Planck constant, v is the frequency. For a given optical band we can determine the direct band gap, or direct gap of semiconductors using n=1/2 and followed by extrapolating the linear region of the graph.

METHODOLOGY

For the development of the work, the sequence in figure 5 was followed.

Figure 5: Methodology followed in the research.

Source: Authors, 2017

3.   RESULTS AND DISCUSSIONS

XRD measurements

The crystal structure of the ZnO particles was characterized by XRD as per Figure 20 where the peaks can be observed. See Figure 6.

To determine the average crystallite size for the ZnO particles using the Scherrer equation, it is necessary to know the value of the instrumental broadening.

The instrumental broadening was acquired through the XRD measurement for a silicon sample. Using the Gaussian, Lorentzian and Pseudo Voigt functions to determine the FWHM of the most intense peak in the diffractogram. For the Lorentzian function FWHM=0.14089°, Gaussian function FWHM=0.1834° and the Pseudo Voigt function FWHM=0.1728°.

Figure 6. Diffractogram of the ZnO particles used in the milling process

Source: Authors, 2017.
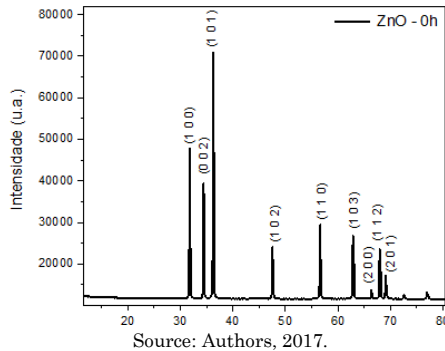
The milling process of the ZnO particles in the first 15 minutes took place with spheres of diameters 2,4,6 and 8 mm considering the BPR (6:1). We can observe in the four diffractograms that the ZnO phase remained stable, that in relation to the diffraction profile of the particles that did not undergo any grinding, the peaks were with their base slightly broadened characteristic of nanometric particles. It is also possible to observe the appearance of a characteristic Fe peak (as per ICSD card: 64998) in the diffractograms of the samples that underwent grinding with the 2- and 6-mm balls.

Figure 7: XRD measurements for the ZnO samples at 15 minutes of grinding.

Source: Authors, 2017.
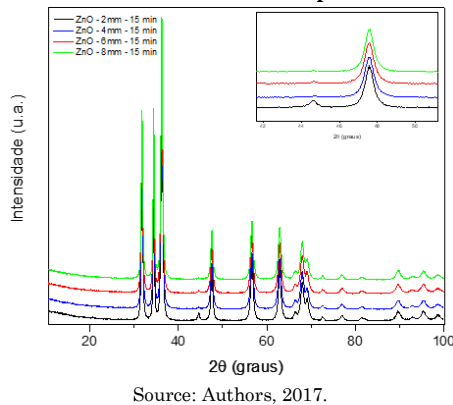
Figure 8 shows the phase identification for the ZnO sample milled with 2 mm balls, where the intensity of the Fe peak is greater. This result can be related to the size of the balls used in the grinding process, as the collisions that occurred during the process allowed for a larger surface area between the balls and the inner walls of the grinding jar. It is also worth noting that

during milling processes it is also important to prevent or minimize contamination of the material caused by the presence of atmospheric air.

Figure 8. Phase identification for ZnO milled 15 minutes with 2 mm beads.
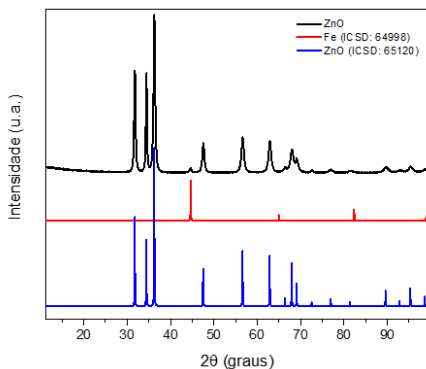
Source: Authors, 2017.

Using the Lorentz, Gaussian, and Pseudo Voigt I function available in the Origin software, the FWHM of the six most intense peaks was determined, where they were subtracted from the instrumental enlargement and the average crystallite sizes were calculated according to tables 1, 2, and 3.

In Figure 9 it is possible to observe the Lorentzian convolution only for the seven most intense peaks and were subtracted from the instrumental broadening, this process occurred with Gaussian and Pseudo Voigt functions.

Figure 9. Convolution of the Lorentzian functions in the diffractogram of the ZnO sample with 7 mm spheres.
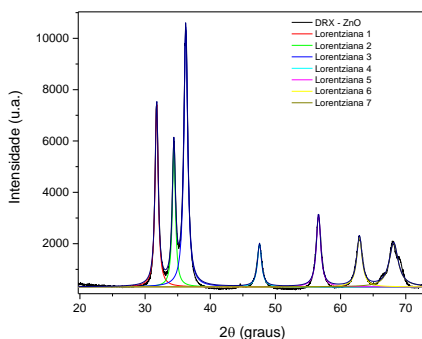
Source: Authors, 2017.

In Figure 10, you have the profiles of the average crystallite sizes as a function of the diameter of the balls, the samples with 15 minutes grinding

showed little variation for the Lorentzian function used to determine the crystallite sizes.

Figure 10. Representation of average crystallite size as a function of bead diameter for samples that underwent grinding for 15 minutes.
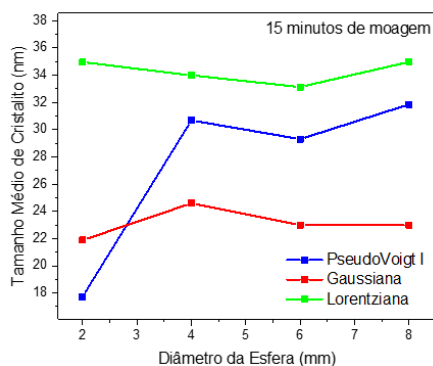
Source: Authors, 2017.

UV/Vis Spectroscopy Measurements

The UV-Vis spectroscopy for the commercial ZnO particles showed maximum absorbance at 379 nm as per Figure 11.

In crystalline materials, the Eopt value is obtained directly from the absorption. In the work of Kakhaki et al, (2015), the optical gap calculation for the band gap of ZnO nanoparticles decreases with increasing average crystallite size. The value of the Gap energy (Eg) for the commercial ZnO particles was obtained by extrapolating the straight line in the graph (αhv)2 versus hv, i.e., the value found is in accordance with the literature.

Figure 11. UV-Vi's spectroscopy for commercial ZnO particles.
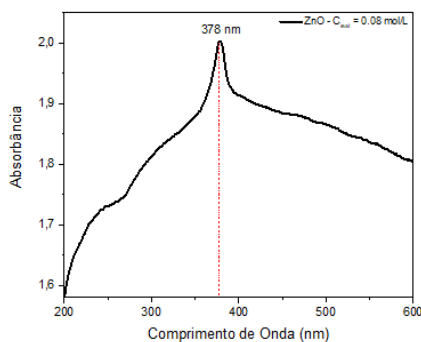
Source: Authors, 2017.

In Figure 12 one can observe the absorbance spectrum for an aqueous solution of commercial ZnO particles with a concentration of 0.08 mg/L, and it was

observed that the peak of maximum absorbance was around 378 nm with calculated gap energy of 3.02 eV. The gap value for ZnO (Wurtzite) nanoparticles is somewhat lower than the values found in the literature that usually report values near 3.2 eV [29, 30, 31].

Figure 12. Plot of (Ahv)^2versus (hv) for commercial ZnO particles
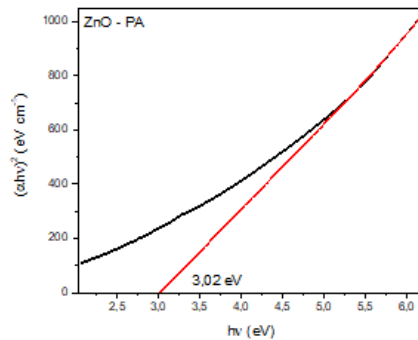
Source: Authors, 2017.

Table 1. Average crystallite size and gap energy information for commercial ZnO and ZnO samples milled for 15 minutes with beads of diameters 2,4,6 and 8 mm.

ZnO 15 minutos de moagem	Tamanho Médio de Cristalito (nm)			Energia de Gap (eV)
	L	G	P	
ZnO Comercial	308	143	192	3.02
2 mm	34,96	21,88	17,72	4,07
4 mm	33,98	24,58	30,68	3,7
6 mm	33,18	22,59	29,30	3,9
8 mm	34,98	22,99	31,85	3,4

Source: Authors, 2017.

For the samples that underwent grinding they had a decrease in average crystallite size and their energy gaps calculated through UV/Vis spectroscopy higher than the gap of commercial ZnO. This increase in the gap band gap is related to the decrease in average crystallite size caused by high-energy grinding. The literature reports that the relationship of the increase in gap energy and the decrease in particle size to the quantum confinement effect [33]. Bagabas et al (2013) relates the increase in gap with Rayleigh scattering [34].

4.   CONCLUSÃO

High energy milling on ZnO particles produced nanostructured samples for different sphere diameters.

The Lorentz, Gaussian, and Pseudo Voigt functions used to determine the broadening of the x-ray diffraction peaks showed a good fit making it feasible to calculate the average crystallite size using the Scherrer equation.

The mean crystallite sizes calculated for the Lorentzian, Gaussian, and Pseudo Voigt functions were very close, i.e., even considering different grinding ball diameters there are no variations in crystallite sizes when keeping the BPR fixed in the grinding process.

The absorbance measurements for commercial ZnO particles allowed a direct gap calculation of the samples through McLean's equation.

The commercial ZnO showed a direct gap of 3.02 eV while for the ZnO samples milled for 15 minutes with the 2,4,6 and 8 mm beads showed an increase in the direct gap values that may be related to the decrease in particle size and Rayleigh scattering.

5.   REFERENCES

[1] NATELSON, D. **Nanostructures and Nanotechnology**. Cambridge University Press, 2015.
[2] COUTO, G. G. **Nanopartículas de níquel: síntese, caracterização, propriedades e estudo de sua utilização como catalisadores na obtenção de nanotubos de carbono.** Dissertação] Programa de Pós-Graduação em Química da Universidade Federal do Paraná, Curitiba, 2006.
[3] AZUMA, F.D. **Síntese e Caracterização de ZnO via Mecanoquímica**. [Dissertação] Universidade Federal do Amazonas, Pós-Graduação em Ciências e Engenharia de Materiais, Manaus, 2016.
 [4] YANHONG, L. et al. **A Study of Quantum Confinement Properties of Photogenerated Charges in ZnO Nanoparticles by Surface Photovoltage Spectroscopy**. The Journal of Physical Chemistry B. v. 108, p. 3202-3206, 2004.
[5] HORBANI, M.; GOLOBOSTANFARDA, M. R.; ABDIZADEH, H. **Flexible freestanding sandwich type ZnO/rGO/ZnO electrode for wearable supercapacitor.** Applied Surface Science 419 (2017) 277–285.
[6] BHATIA, S. and VERMA, N. **Photocatalytic activity of ZnO nanoparticles with optimization of defects**. Materials Research Bulletin 95, (2017) 468-476.
[7] HEO, Y.W. et al. **ZnO Nanowire Growth and Devices**. Materials Science and Engineering Review, v. 47, p. 1-47, 2004.
[8] SENDI, R.K. and MAHMUD, S. **Quantum size effect on ZnO nanoparticle-based discs synthesized by mechanical. Milling**. Applied Surface Science 258 (2012) 8026– 8031.
[9] DAMONTE, L.C.; DONDERIS, V.; HERNÁNDEZ-FENOLLOSA, A. **Trivalent dopants on ZnO semiconductor obtained by mechanical milling**. Journal of alloys and compounds 483 (2009) 442-444.
[10] SUWANBOONA, S. and AMORNPITOKSUKB, P. **Preparation of Mg-doped ZnO nanoparticles by mechanical milling and their optical properties**. Procedia Engineering 32 (2012) 821 – 826.

[11] GHORBANI, M.; GOLOBOSTANFARD, M.R. and   ABDIZADEH, H. **Flexible Freestanding Sandwich Type ZnO/rGO/ZnO Electrode for Wearable Supercapacitor**, Applied Surface 419 (2017) 277–285.

[12] HARRIS, J.R.; WATTIS, A.D.; WOOD, J.V. **A comparison of different models for mechanical alloying**. Acta Mater (2001) 3991-4003.

[13] LU, L. and LAI, M.O. **Mechanical Alloying**, Kluwer Acad Publishers, Boston, MA, 1998.

[14] TIAN, Z.Y.; CHEN, Y.; YANG, W.S.; YAO, J.N.; ZHU, L.Y.; SHUAI, Z.G. **Angew. Growth, morphology and optical properties of tris**, Chem. 116 (2004) 4152.

[15] BHADESHIA, Ligas **ODS Práticas, Ciência de Materiais e Engenharia** A, 223 (1997) 64-77.

[16] GUINEBRETIÉRE, R. X-ray **Diffraction by Polycrystalline Materials**. First Edition, ISTE Ltd, 384 p., 2007.

[17] SURYANARAYANA, C. **Mechanical alloying and milling**. Marcel Dekker, New York, 492p., 2004.

[18] SOPICKA-LIZER, M. **High-energy ball milling Mechanochemical processing of nanopowders**. First Edition. 440 p., 2010.

[19] SURYANARAYANA, C., et al. **The science and technology of mechanical alloying**. Materials Science and Engineering A, v. 304-306, p. 151-158, 2001.

[20] BHADESHIA, Ligas **ODS Práticas, Ciência de Materiais e Engenharia** A, 223 (1997) 64-77.

[21] MAIA, A.O.G., **Sinterização de Nanopartículas de NiO por gelatina Comestível**. [Dissertação] Universidade Federal do Ceará, Pós-Graduação em Física, Fortaleza, 2005.

[22] REISDOERFER, E.C., **Síntese e Caracterização do sistema ZnO-FeO submetido à moagem de alta energia**. [Dissertação] Universidade Estadual de Maringá, Pós-graduação em Física, Maringá, 2008.

[23] TREVIZO, A.S.; MADRID, P.A.; RUIZ, P.P.; FLORES, W.A. and Yoshida, M.M. **Optical Band Gap Estimation of ZnO Nanorods**. Materials Research, 16 (2016) 33-38.

[24] POFFO, C.M. LIMA, J.C. S.M. SOUZA., GRANDI, T.A. de BIASI, R.S. **Structural, thermal, optical and photoacoustic study of nanostructured FeSb2 prepared by mechanical alloying**. Physica B 413 (2013) 47-54.

[25] CAGLAR, M.; CAGLAR, Y. and ILICAN, S. **The determination of the thickness and optical constants of the ZnO crystalline thin film by using envelope method**. Journal of optoelectronics and advanced materials, v.8, no. 4 (2016)1410 – 1413.

[26] NAIR, A.S. and ISAC, J. **Effect of Temperature on Optical Properties of Nanocrystalline Ceramics Fe2Mn2Ni2Zn2O11**. International Journal of Science and Research v. 4 Issue 6, (2015) 1562 – 1567.

[27] RUSDI, R.; RAHMAN, A.A.; MOHAMED, N.R.; KAMARUDIN, N. and Kamarulzaman, N. **Preparation and band gap energies of ZnO nanotubes, nanorods and spherical nanostructures.** Powder Technology 210 (2011) 18–22.

[28] KUMAR, H. and RANI, R. **Structural and Optical Characterization of ZnO Nanoparticles Synthesized by Microemulsion Route**. International Letters of Chemistry, Physics and Astronomy 14 (2013) 26-36.

[29] BAGABAS, A.; ALSHAMMARI, A. ABOUD, M.F. and KOSSLICK. H. **Room-temperature synthesis of zinc oxide nanoparticles in different media and their application in cyanide photodegradation.** Nanoscale Research Letter 8:516 (2013) 10p.

[30] SARMA, B and SARMA, B.K. **Role of residual stress and texture of ZnO nanocrystals on electro-optical properties of ZnO/Ag/ZnO multilayer transparent conductors**. Journal of Alloys and Compounds, 734, (2018) 210–219.

[31] ACUÑA, K. YAÑEZ, J.; RANGANATHAN, S.; RAMIREZ, E.; CUEVAS, J.P.; MANSILLA, D.; SANTANDER, P. **Photocatalytic degradation of roxarsone by using synthesized ZnO nanoplates.Solar Energy** 157 (2017) 335-341.

[32] POFFO, C.M. LIMA, J.C. S.M. SOUZA., GRANDI, T.A. de BIASI, R.S. **Structural, thermal, optical and photoacoustic study of nanostructured FeSb2 prepared by mechanical alloying**. Physica B 413 (2013) 47-54.